A novel bistable energy harvesting concept

G. Scarselli* F. Nicassio* F. Pinto† F. Ciampa† O. Iervolino† M. Meo†
*Universitá del Salento, † University of Bath

Abstract

Bistable energy harvesting has become a major field of research due to some unique features for converting mechanical energy into electrical power. When properly loaded, bistable structures snap-through from one stable configuration to another, causing large strains and consequently power generation. Moreover, bistable structures can harvest energy across a broad-frequency bandwidth due to their nonlinear characteristics. Despite the fact that snap-through may be triggered regardless of the form or frequency of exciting vibration, the external force must reach a specific snap-through activation threshold value to trigger the transition from one stable state to another. This aspect is a limiting factor for realistic vibration energy harvesting application with bistable devices. This paper presents a novel power harvesting concept for bistable composites based on a "lever effect" aimed at minimising the activation force to cause the snap through by choosing properly the bistable structures' constraints. The concept was demonstrated with the help of numerical simulation and experimental testing. The results showed that the actuation force is one order of magnitude smaller (3-6%) than the activation force of conventionally constrained bistable devices. In addition, it was shown that the output voltage was higher than the conventional configuration, leading to a significant increase in power generation. This novel concept could lead to a new generation of more efficient bistable energy harvesters for realistic vibration environments.

Keywords: Bistable Composites, Energy Harvesting, Power Generation, Smart materials.

1. Introduction

Energy harvesting systems have been deeply investigated in the last few years for a wide variety of applications ranging from self-powered microsystems to bigger scale and

more complex devices. Several micro-energy harvesting sources can be identified, including motion, vibration (or mechanical energy), electromagnetic and pressure gradients ([1], [2]). Regardless of the conversion mechanism, power harvesting systems are generally designed to operate optimally at or very close to resonance but their efficiency decreases considerably with frequency-varying and wideband vibrations. To address this issue, researchers have proposed different strategies to increase the operating frequency range of vibration energy harvesters [3]: a possible solution can be the periodic tuning of the resonant frequency of the power generator so that it matches the frequency of the ambient vibration. Periodic tuning can be achieved using mechanical or electrical methods. Bandwidth widening can be also obtained using a generator array, a mechanical stopper, nonlinear (e.g. magnetic) springs or "bistable structures". Potential interesting applications for power harvesting come, indeed, from the employment of bistable materials. Particularly, the activation of a snap-through mechanism in bistable systems allows the transition from one stable state to another. This causes large amplitude motion and an increase of power generation [4]. Due to their nonlinear characteristics, bistable devices may be effective across a broad frequency bandwidth. Additionally, snap-through may be triggered regardless of the form or frequency of exciting vibration, thus alleviating concerns about harvesting performance in many realistic vibratory environments dominated by effectively low-pass filtered excitation [5]. In Ferrari et al. [6] a piezoelectric cantilever beam was coupled to two permanent magnets with opposite polarities to create a bistable system: under proper conditions the system bounced between two stable states in response to random excitations. In Stanton et al. [7] a similar bistable energy harvester consisted of discontinuously laminated piezoelectric beam with a nonlinear boundary condition

imposed by repelling permanent magnets. One permanent magnet was at the free end of the cantilevered beam with opposite polarity of a fixed magnet located nearby. The base excitation of the clamping mechanisms of the beam represented an environmental vibration: at a critical separation distance, the elastic restoring force of the beam was overcome by magnetic repulsion, forcing the cantilever to deflect into one of the two potential wells. Piezoelectric laminates bonded to cantilever beam represent one of the more efficient mechanisms for energy conversion [8] and the experiments performed in [6], [7] and [9] verified the efficiency of this type of nonlinear bistable harvesters over a large frequency and amplitude range. Harne and Wang [4] performed a comprehensive review of the different types of bistable harvesters concluding that they are an improvement upon their linear counterparts in steady-state vibration environments. In Arrieta et al., [10] and [11], the nonlinear behaviour of a bistable composite plate with bonded piezoelectric patches was exploited for broadband nonlinear energy harvesting such as the one proposed in the present work.

However, the main problem associated with the bistable concept is that, even under the assumption of optimal excitation frequency and wide-band capability of the bistable energy harvester, a low magnitude force would not generate the nonlinear elastic snap-through mechanism. This activation force has a threshold value that is strongly dependent on the materials used, layup, curing cycle, geometry and boundary conditions. The decrease of the activation force leads to more efficient energy harvesters.

This work presents a novel bistable energy harvesting concept aimed at obtaining a more efficient snap-through solution reducing the activation force, thus allowing harvesting energy of an order of magnitude higher than what obtained in literature. In

particular, a “lever effect” concept was introduced to optimise the performance of a power harvesting system based on the employment of a bistable composite plate constrained in a proper way. This “lever effect” showed that the activation force needed for the transition from a stable state to another (i.e. the snap-through behaviour) was significantly lowered and strongly dependent on the boundary conditions. A coupled thermal-structural finite element (FE) model was implemented in order to compare post-cure deformation shapes and the actuated deformation of the composite laminate. Experimental tests were carried out to validate the numerical-analytical models by constraining the bistable plate in a specifically designed multifunctional frame. A piezoelectric sensor was bonded onto the surface of the bistable plate in order to scavenge energy during the transition between the two stable states that can be optimised by selecting ad-hoc boundary conditions. The main finding of this work is that for a bistable plate the same configuration of constraints that minimise the activation force for the snap-through, will then maximise the output energy from the piezoelectric sensor. In this way an enhanced power harvester with a high level of efficiency (i.e. ratio between output energy and input energy) can be obtained.

2. Enhanced energy harvesting with snap through plate: the lever effect

The bistable plate as a first approximation can be idealised as a beam. In order to minimise the snap through activation force from one stable state to another one, the following concept as illustrated in the Figure 1 has been developed.

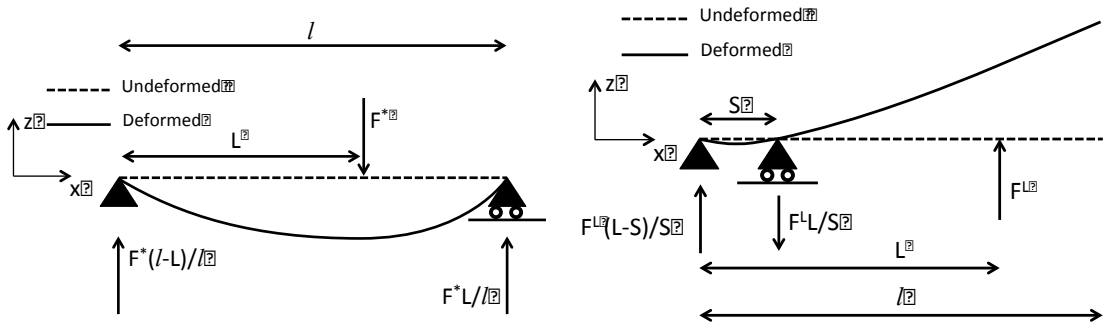

Figure 1: Beam deformation with simple supports (left) and with lever (right).

The concept uses the "leverage effect" to be applied to the snap-through in order to activate the transition between the stable states: lower forces (F^L) are able to originate big deformations when the constraints are properly applied (Figure 1). The transition is activated by external forces as soon as the deformation energy reaches a proper threshold. It is possible to demonstrate that this activation force strongly depends on the constraints lay-out. If the beam is simply supported at the ends and loaded by a point load along the span in a point of coordinate *L*, the constraint forces and the moment follow the scheme represented in Figure 2.

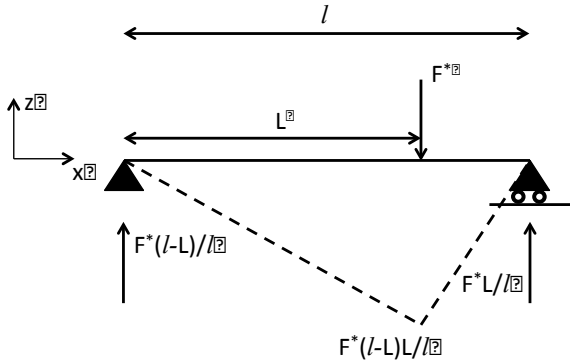

Figure 2: Free body diagram of specimen loaded along the span and simply supported at the ends.

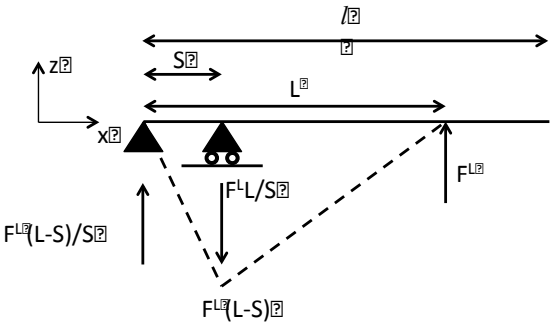

Figure 3: Free body diagram of bistable specimen loaded at the end and simply supported (lever).

The deformation energy for the structural scheme in Figure 2 is:

$$U_1 = \int_0^L \frac{M(x)^2}{2EI}\, dx = \int_0^L \frac{\left(\frac{F(l-L)}{l}x\right)^2}{2EI}\, dx = \frac{F^2\left(1-\frac{L}{l}\right)^2 L^3}{6\,EI}$$

$$U_2 = \int_0^{(l-L)} \frac{M(x)^2}{2EI}\, dx = \int_0^{(l-L)} \frac{\left(\frac{FL}{l}x\right)^2}{2EI}\, dx = \frac{F^2(1-\frac{L}{l})^2 b^2 (l-L)}{6\,EI} \tag{1}$$

where *M(x)* is the bending moment, *E* the Young's modulus, *I* the cross sectional moment of inertia, *l* the length of the beam, U_1 and U_2 are respectively the deformation energy of the part of beam with the coordinate *x* ranging between 0 and *L* and between *L* and *l*. The total deformation energy is therefore:

$$U^* = U_1 + U_2 = \frac{F^{*2} b^2 (1-\frac{L}{l})^2 l}{6\,EI} \underset{L=Bl}{\Longrightarrow} U^* = \frac{F^{*2} l^3 B^2 (1-B)^2}{6\,EI} \tag{2}$$

where $L = Bl$ and *B* is a non-dimensional parameter between 0 and 1. As U* reaches the threshold, the transition of the bistable plate from a configuration to another one occurs. To minimize the activation force, a support is introduced at a coordinate *a* between the point load and the support at the other end (lever). Reaction forces and moment diagram follow the scheme represented in Figure 3. In this case the total deformation energy is evaluated as follows:

$$U_1 = \int_0^S \frac{M(x)^2}{2EI}\, dx = \int_0^S \frac{\left(\frac{F(L-S)}{S}x\right)^2}{2EI}\, dx = \frac{F^2(L-S)^2 S}{6\,EI}$$

$$U_2 = \int_0^{(L-S)} \frac{M(x)^2}{2EI}\, dx = \int_0^{(L-S)} \frac{(Fx)^2}{2EI}\, dx = \frac{F^2(L-S)^3}{6\,EI} \tag{3}$$

and expressing the length *S* as a fraction *A* (between 0 and 1) of *l*:

$$U^L = U_1 + U_2 = \frac{F^{L^2} L(L-S)^2}{6\,EI} \underset{L=Bl}{\overset{S=Al}{\Longrightarrow}} U^L = \frac{F^{L^2} l^3 B(B-A)^2}{6\,EI} \tag{4}$$

Under the assumption that the threshold deformation energy necessary to move from one stable state to another remains the same between the analysed configurations (Figure 2 and Figure 3), the following equations holds:

$$U^L = U^* \Rightarrow \frac{{F^L}^2 l^3 B(B-A)^2}{6\,EI} = \frac{{F^*}^2 l^3 B^2 (1-B)^2}{6\,EI} \Rightarrow \frac{F^L}{F^*} = \frac{\sqrt{B}(1-B)}{(B-A)} \tag{5}$$

in which the ratio between the two activation forces is expressed as a function of the two non-dimensional parameters *A* and *B* (both ranging between 0 and 1). The activation force ratio is plotted in Figure 4 where only values of *B* bigger than *A* were considered, i.e. the activation force F^L is never applied between the two supports. To minimize this function, *B* should approach 1 and *A* should approach 0. It must be remarked that *A* cannot be equal to 0 since the two supports cannot be the same. It is clear that the activation force F^L can be reduced respect to F^* by choosing properly *A* and *B*. This graph shows that it is possible, by choosing an appropriate set of A and B, to significantly lower the snap-through activation force and achieve a more efficient and stable power harvesting system.

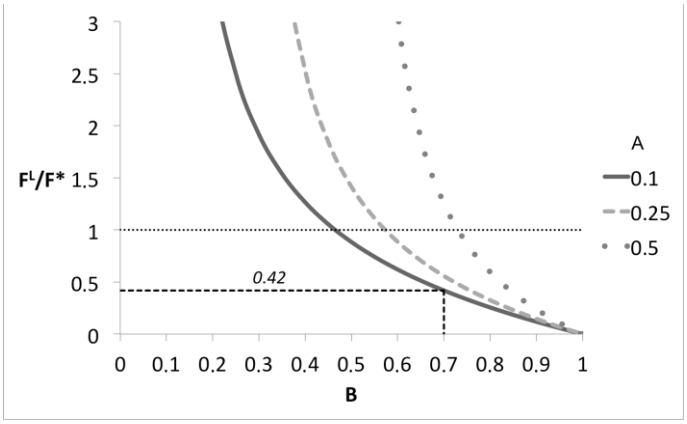

Figure 4: Activation force ratio as a function of A and B.

As an example, in Figure 4 it is highlighted the case of A = 0.1 and B = 0.7. From this figure, it is clear that ratio between the activation forces is 0.42. The lever effect allows,

in this case, to save 58% on the force needed for the transition between the stable states.

3. Modelling of the snap through process

A numerical FE model was developed (i) to simulate the structural behaviour of bistable plates in order to numerically obtain the activation forces and to design the experiments and (ii) to evaluate the deformations at each point over the plate surface in order to properly choose the sensors placement for power harvesting. The numerical analysis was split up in two load cases: the thermal simulation to induce the curved shape and the transient dynamic simulation of the snap through-deformation. The commercial software ANSYS® 15.0 was used [12]. The bistable rectangular plate (240mm × 120mmx0.5mm) is made up of asymmetric laminates and stacking sequence of $[0_2/90_2]$. The material used was T800/M21 (see [13] for the elastic properties). For the first load case (cooling down), the goal was to simulate the deformed shape due to the thermal residual stresses. The temperature profile applied to the mesh nodes was a linear ramp from 150 °C to 15 °C. For the transient analysis, the panel was modelled using 480 SHELL181 elements and 527 nodes [14], with each node having six degrees of freedom. Convergence studies on the mesh size were carried out in order to determine acceptable accuracy of the model and good time-solving. The option “Large Deflection” was employed in each step because of large deformation for small load increments of the plate during the process (geometric non-linearity). A transient structural analysis was performed to simulate the cooling-down and the snap-through mechanism. A total duration of 1 s and 10 s were assumed for the cooling down and the snap-through, respectively. Each time was then divided into smaller time steps. The cooling down was

solved with a time step of 0.1 s, whereas the bistable activation was solved tuning the time step according to the deformation gradient. Particularly, for low deformation gradients (small increases of applied force cause small increases of deformation of the structure) the time step was 0.1 s, whilst for high deformation gradients (small increases of applied force cause big increases of deformation of the structure) the time step was set at 0.001 s. In this way, the convergence is guaranteed for each time step. Convergence is also depending on the boundary conditions: two simple supports on the middle nodes on the short sides of the rectangular plate and two rotational constraints on the same nodes along direction "y" (see Figure 5 for directions x, y and z) were applied. The numerical results are reported in Table 1 and compared with the experimental results. An error less than 9% was found for all the stable configurations.

	Simulated Camber [m]	**Measured Camber [m]**	**Error [%]**
1st stable shape	6.17×10^{-3}	6.28×10^{-3}	1.75
2nd stable shape	19.81×10^{-3}	18.22×10^{-3}	8.73

Table 1: Simulated and measured cambers

Then, in order to evaluate the threshold forces needed to activate the snap-through mechanism, nonlinear transient structural simulations were carried out.

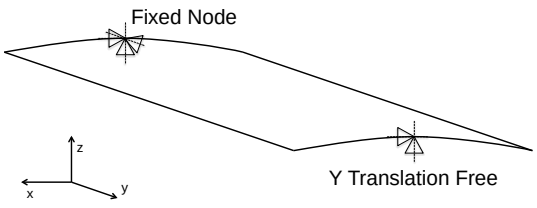

(a) Sample supported on short side (Configuration 1)

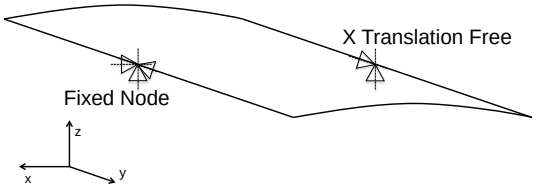

(b) Sample supported on long side (Configuration 2)

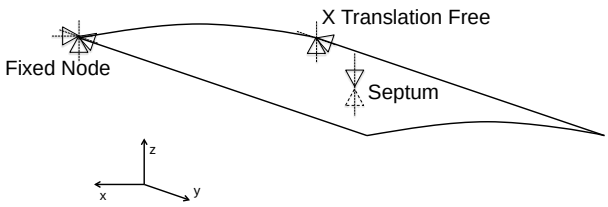

(c) Variable septum position

Figure 5: Illustration of boundary conditions on the bistable composite panel.

Various load cases were analysed to study the bistable behaviour in different boundary conditions and activation force positions as shown in Figure 5 (each triangle represents the constraint to the displacement in that direction).

Typical bistable deformations and snap through transition between state 1 and state 2 and vice versa are shown in Figure 6 and Figure 7. The contours help to realise that each side, for both the stable states, has a curvature as stated by Gauss in his "Theorema Egregium" [15]. The theorem says that the Gaussian curvature of a surface (the product of the principal curvatures at a point) is an intrinsic invariant. In the bistable composite plate under investigation, the Gaussian curvature is strictly negative in both stable shapes since the two principal curvatures are of opposite sign. The unstable state, at the transition between two stable states, is a saddle, which is a peculiar geometry with negative Gaussian curvature [16].

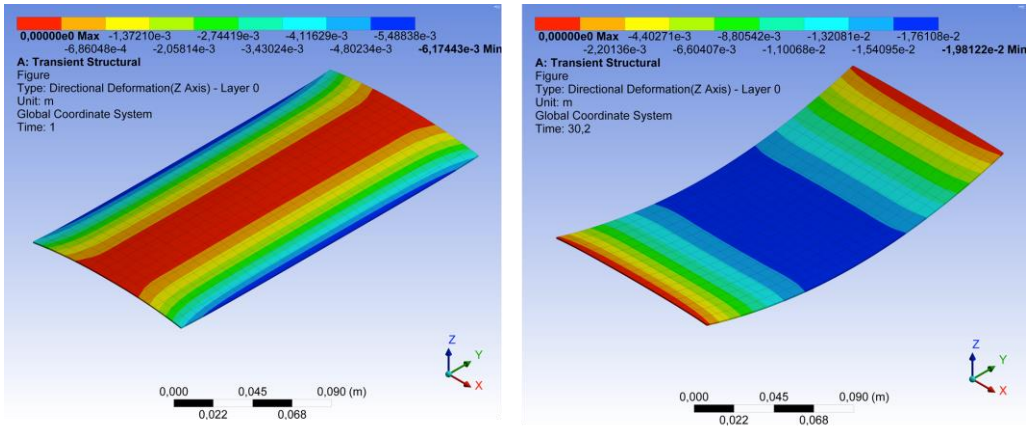

Figure 6: Bistable panel model and the two stable state shapes.

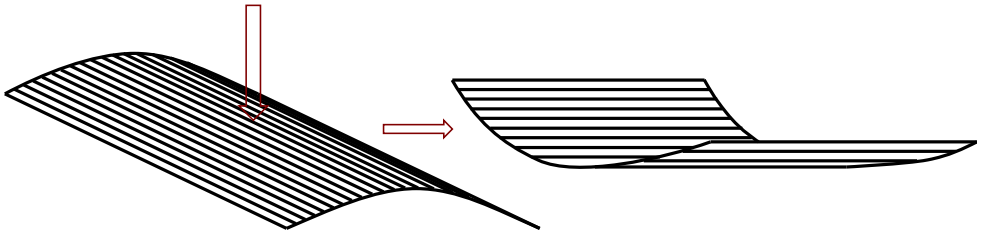

a) Snap through from stable state 1 to stable state 2

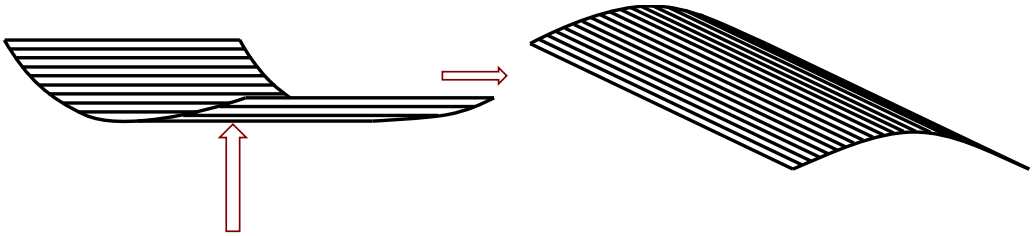

b) Snap through from stable state 2 to stable state 1

Figure 7: Snap through transition.

Figure 8: Time history of snap-through

Figure 8 reports the time history of the deformed shapes of the bistable plate at each time step of the structural analysis. The time “1 s” refers to the cooling down with the

configuration 1 of constraints (Figure 5a). Then, the point load application with the use of the septum and of new constraints is simulated until the snap through is activated.

The numerical results provided by the thermal and structural FE models allow to define (i) the activation forces for the transition from a stable state to the other one that will be compared with the experimental results in the following paragraphs and (ii) the deformations at each point over the surface of the sample for power harvesting purposes. The simulations showed that the membrane deformations along direction "*y*" (see Figure 5) on the top surface of the bistable sample are more or less constant in the region between the septum and the free end of the plate: for S = 40 mm, L = 240 mm (see Figure 11) and an activation force of 1.85 N from state 1 to state 2, the order of magnitude of such deformation is 4×10^{-3} mm/mm. The membrane deformation along direction "*x*" was one order of magnitude smaller ($\sim 10^{-4}$). These results suggested to place a Micro Fibers Composite (MFC) sensor near the free end of the bistable plate in order to exploit the membrane deformation along the direction "*y*" and to move the septum along and over the sample for the experiments.

4. Experimental Set-up

The numerical simulation results showed that a significantly lower force was needed to activate the snap-through by exploiting the "lever effect". In order to find experimentally the forces required to activate this mechanism, a number of four-layer asymmetric CFRP laminates was fabricated. The nominal thickness of the initial carbon pre-preg sheet was 0.125 mm, and the total laminate thickness was 0.5 mm. The rectangular shape of the laminates was chosen in order to enhance the asymmetry between the 0 and 90 degrees oriented plies, thus increasing the achievable curvature

during the curing reaction. Samples were cured in autoclave using two different curing cycles in order to study the relation between curing temperature and activation forces. The effect of the sample-curvature on a bistable composite laminate was analysed by a number of authors. Examples are Giddings et al. [17] and Msallem et al. [18]. Based on their studies and the information provided by the producer of the pre-preg used in this research work, the authors chose a curing cycle at lower temperature in order to reduce the force required for the snap-through activation. In particular, the samples manufactured with a lower temperature profile were compared with the samples manufactured using the standard temperature profile at 180°C. As explained throughout the paper, the authors analysed the sample cured at lower temperature (150°C) in order to obtain the higher effectiveness of the system. Indeed the force required for the snap-through activation is lower for the sample cured at lower temperature with respect to the sample cured following the prepreg producer instruction (see Table 2). The first sample was cured following the traditional cycle suggested by the producer, setting the temperature at 180°C with a rate of 5 °C/min, while a second batch was prepared at 150°C (with a rate of 5 °C/min) with the overall curing cycle of 3 hours. In order to increase the generated stresses and obtain a higher level of curvature in the samples, both laminates were removed from the autoclave immediately after the curing reaction and rapidly cooled down in open air instead of following the cool rate of 2-5 °C/min suggested by the manufacturer. The maximum cambers in the two stable shapes are reported in Table 2. Upon cooling to room-temperature, the manufactured laminates were observed to have two stable states of curvature. The curvatures are due to a mismatch in the thermal expansion behaviour of

the layers within the laminate. These particular characteristics are common in asymmetric laminates when subjected to a thermal field that varies with time [19] [20].

	Sample 1 **Curing Temperature 150 °C**		**Sample 2** **Curing Temperature 180 °C**	
Maximum Camber	Stable state 1	Stable state 2	Stable state 1	Stable state 2
	6.28 mm	18.22 mm	7.60 mm	19.50 mm

Table 2: Maximum camber at different curing temperatures.

The snap through mechanism between the two stable shapes is activated with a small energy input.

Large achievable displacements and low energy requirements are the main reasons for the increasing interest about bistable composite laminates, in particular for applications such as morphing structures [21] and energy harvesting.

The actuation force required to activate the snap through mechanism is highly dependent on the degree of the laminate curvature, the material properties and the curing cycle. Indeed, for the sample cured at 180 °C, the force required to shift between the two different stable configurations is higher with respect to the laminate cured at 150 °C. Moreover, as stable state 2 is characterised by a maximum camber higher than stable state 1 (see Figure 7), the force required to activate the snap through mechanism was lower for the 2-1 transition than the one required for the inverse movement 1-2. In order to obtain a higher effectiveness of the system, the sample cured at lower temperature was chosen for the experimental set-up. To scavenge energy from the transition between the two plate-states, a MFC sensor was bonded with epoxy resin onto the surface. A MFC sensor is a piezo-device (see [22] and [23]) that can be used to harvest energy from vibrations with a broadband operation bandwidth ranging between 0 – 1 MHz [24]. This sensor was connected to a Picoscope (oscilloscope) with a sampling frequency of 20 kHz. The acquisition window of the measured signals was 150 ms. A

Polytech laser vibrometer was also used to measure the out-of-plane accelerations of the plate.

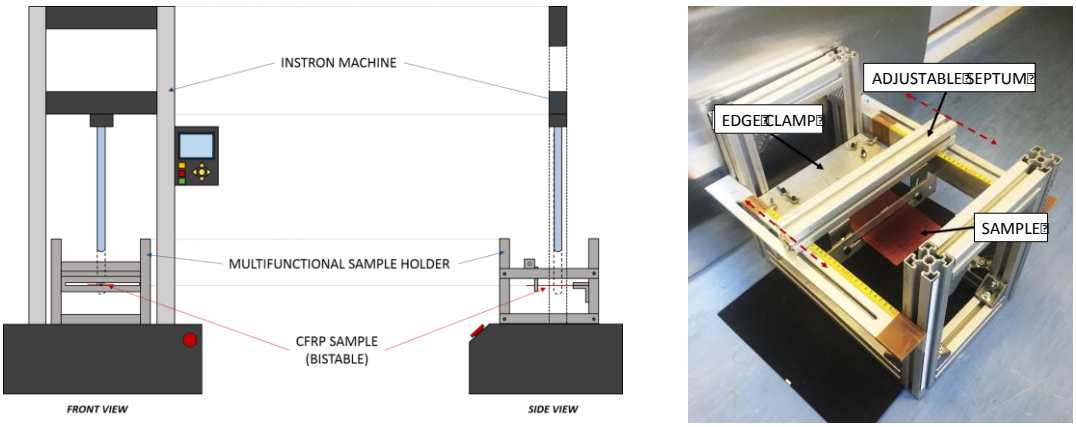

Figure 9: Snap through force evaluation test setup.

The activation forces were evaluated by carrying out specific tests represented in Figure 9. A multifunctional sample holder was manufactured by a frame made with t-slotted aluminium profiles equipped with two moving parts on rails so that it is possible to adjust each side of the support structure and fix one edge of the sample with a clamp. A septum (representing the fulcrum of the lever) can be regulated along the entire length of the aluminium profile in order to move a support constrain. Comparing Figure 9 with Figure 5, it can be noticed that the “Edge Clamp” (see Figure 9) allows to constrain the short edge of the bistable sample: the left node of the short side is fixed, the right one can shift along X direction. The “Adjustable Septum” can shift along Y direction. As a result, the final configuration can be described as a hyperstatic simply supported cantilever plate.

5. Experimental results

The activation forces experimentally obtained in several configurations of constraints are here analysed and discussed. The Instron® machine was set in order to operate in "steady-state" mode due to the very low probe's speed (maximum 50*mm*/*min*). The bistable plate was loaded at the centre and was constrained as shown in Figure 5(a) and Figure 5(b). Because the Instron® machine measures the plate reaction force, the load curves in Figure 10 show a maximum value after an almost linear behaviour. The reaction force then decreases immediately after the maximum value due to a redistribution of internal stresses during the snap-through phenomenon. Two configurations are shown. For the configuration of constraints 1 the average activation forces to reach the first and the second stable shape are equal to 32.3 *N* and 6.0 *N* respectively. The activation forces for the configuration of constraints 2 are very similar each other: 16.5 *N* to reach the first shape and 15.4 *N* for the second one.

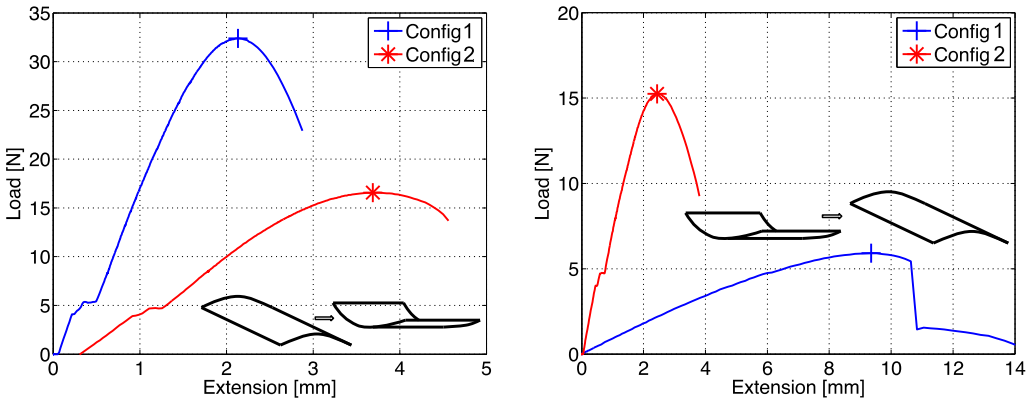

Figure 10: Activation forces in configuration 1 and 2

The interaction between the constraints and the composite fibres are the reasons that explain such important difference in activation forces: the force to activate the second stable state in configuration 1 is the biggest one because it has to work against the shorter 90° fibres to bend the longer 0° fibres, while the smallest force to activate the

first stable state in configuration 2 has to work against the longest fibres to bend the shorter ones. The activation forces in configuration 2 are very similar because both snaps through are activated by 0° fibres deformation. These two preliminary experimental results were used as a reference for the following experimental tests since they provided the activation force pattern and values in two specific configurations of constraints not exploiting the "lever effect". This effect was introduced and tested with the sample holder shown in Figure 9, which allowed to move the septum and the load application point.

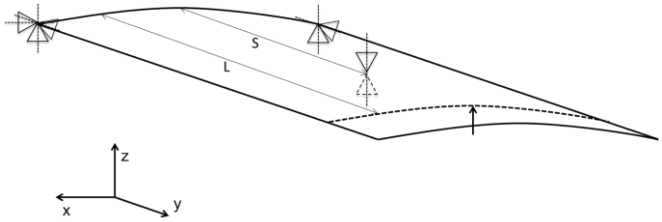

Figure 11: S (septum position) and L (load position)

Figure 11 shows the septum and load positions: "S" indicates the distance in mm of the septum position, whilst "L" indicates the distance in mm of the load position. Several configurations of boundary conditions and loads for transition from stable state 1 to stable state 2 were not investigated and not reported because they were not suitable for the adopted experimental set-up: these configurations of boundary conditions and force locations were, indeed, strongly unstable: in other words, the transition of bistable occurred even with small perturbations and without force application. Figure 12 illustrates the experimental results associated to the activation forces acquired for different configurations of load and constraints, resulting in different values of "S" and "L". The curves in Figure 12 show a trend similar to the ones represented in Figure 10, i.e. they drop notably after the maximum is reached. The drops are directly proportional to the value of the maximum force. Similarly to the previous configuration of constraints

reported in Figure 10, it can be noticed that the force needed for activating the transition between state 2 and state 1 is lower than the one needed for the transition between state 1 and state 2. This difference vanishes when the "lever effect" is exploited since the activation forces become small and of similar magnitude. For both the transitions between the two stable states, a minimum activation force can be determined, which is marked in Figure 12 with a circle, corresponding to a specific value of "S" and "L".

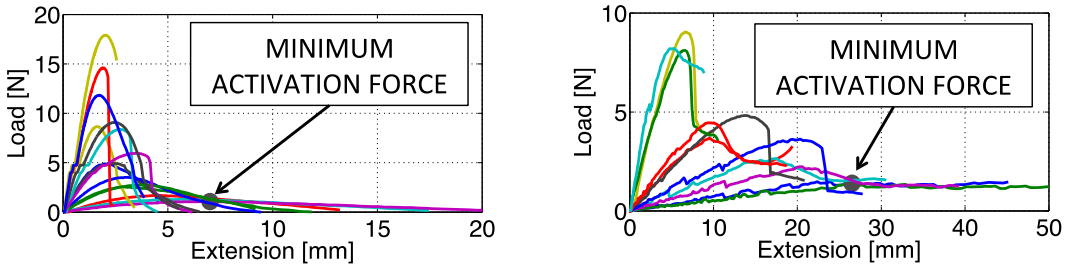

a) Transition between stable state 1 and stable state 2 b) Transition between stable state 2 and stable state 1

Figure 12: Activation forces with variable position of load "L" and septum "S".

Figure 13 was plotted comparing the maximum value of load for each combination of "S" and "L", which corresponds to the activation force. This figure depicts the following important result: the actual activation force responsible for the transition between the two stable states decreases with shifting the application point towards the free edge (i.e., increasing "L") and the septum position towards the constrained edge (i.e., decreasing "S"). The optimal configuration which generates the lowest combination of snap-through forces is the one with septum position S = 40 mm and load position L = 240 mm. The "lever effect" is the explanation of these results: i.e. by maximising the distance between the fulcrum and the load position, it is possible to obtain the same effect using a reduced activation load. For the configuration with S = 40 mm and L = 240 mm it was experimentally found that the transition from the stable state 1 to the stable state 2 was activated by a force of 1.08 N and the transition from the stable state 2 to

the stable state 1 was activated by a force of 1.10 N. In the following Table 3 the results are summarised for the different configurations of constraints taken into account: it is clear that the best configuration with S = 40 mm and L = 240 mm allows to activate the snap-through with a force much lower than the force needed for configurations 1 and 2.

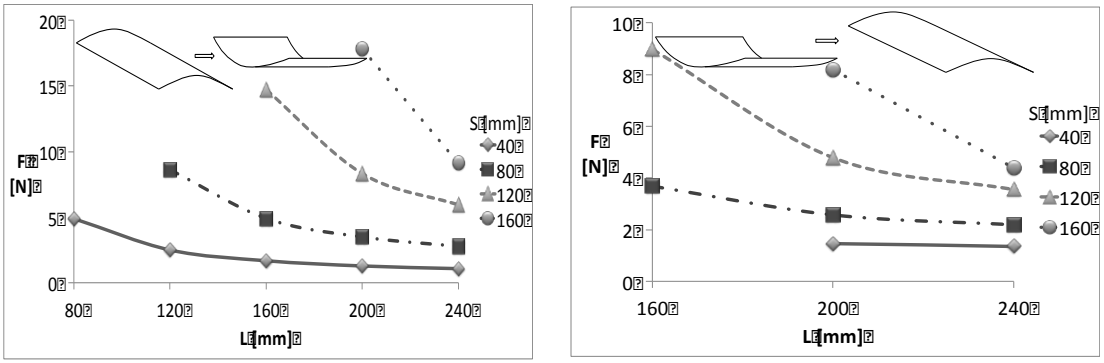

a) Transition between stable state 1 and stable state 2

b) Transition between stable state 2 and stable state 1

Figure 13: Activation forces with variable positions of septum (S) and loads (L)

For example, the force needed for the transition between the state 2 and the state 1, with the exploitation of the lever effect, is only the 3.4 % of the force needed in configuration 1 and only the 6.7 % of the force needed in configuration 2.

Force [N]	Configuration 1	Configuration 2	Lever	Lever as a percent of Configuration 1	Lever as a percent of Configuration 2
From State 1 to State 2	6.0	15.4	1.08	18.0 %	7.0 %
From State 2 to State 1	32.3	16.5	1.10	3.4 %	6.7 %

Table 3: Activation forces comparison between different configurations of constraints

These results are very promising and confirm the validity of the proposed approach specially if compared with the data available in literature. As an example, in Fuhong et al. [25], the bistable activation force (~1.33 N) for a panel with thickness of 0.23 mm (nearly half of the thickness of the panel tested in this paper) and different constraints,

was of the same order of magnitude as the activation force found for the bistable composite laminate tested in this paper. Similarly, in Mattioni et al. [26], the bistable panel with the same thickness of 0.5 mm, was activated by a force about four times greater (4.65 N) than the activation force found in this paper and, also in this case, the structural constraints were different.

6. Experimental/numerical correlation

The FE model simulates the structural behaviour of the plate with some differences due to boundary conditions and applied load: supports were assumed perfect, cylindrical and without friction. Indeed during each experiment, the Instron probe applied the force on different points over the plate surface because of composite large deformations, while in the FE model the activation force was acting always on the same node during the entire analysis. Furthermore, at the transition between the two stable states, inertial effects are not sensed by the Instron probe as the plate accelerates and loses contact with the load cell. These inertial terms must be added to the loads read by the Instron to make a comparison with numerical activation loads. These discrepancies cause errors between the experimental activation forces and the numerical ones, as represented in Table 4. The laser vibrometer provided the acceleration values at different points of the sample surface at the snap-through. These values were used to evaluate the inertial forces to be added to the loads read by the Instron test machine in the case when the probe has lost the contact with the sample (Case 1, 3 and 5 of the Table). When the probe did not lose contact with the sample (Case 2, 4 and 6), accelerations were not used, no inertial effects were considered and there was a good agreement between the numerical and experimental activation forces. It is clear from the Table 4 that, taking

properly into account the inertial effects, a reasonable agreement between the numerical model and the experiments could be achieved.

Case	Instron Load [N]	Acceleration [m/s^2]	Inertial Load [N]	Tot Act Load [N]	Ansys Load [N]	Error [%]
1	16.30	182	8.01	24.31	23.20	4.56
2	32.30	-	-	32.30	32.90	1.86
3	15.30	188	8.27	23.57	22.10	6.24
4	6.00	-	-	6.00	6.19	3.17
5	1.08	17	0.62	1.70	1.85	8.61
6	1.10	-	-	1.10	1.01	8.18

Table 4: Experimental/numerical correlation (Case 1: transition from state 1 to state 2 in configuration of constraints 2; Case 2: transition from state 1 to state 2 in configuration 1; Case 3: transition from state 2 to state 1 in configuration 2; Case 4: transition from state 2 to state 1 in configuration 1; Case 5: optimal combination of S=40 mm and L=240 mm and transition from state 1 to state 2; Case 6: optimal combination of S=40 mm and L=240 mm and transition from state 2 to state 1).

7. Power Harvesting Performance

In order to measure the capability to harvest energy for the proposed harvester, a MFC sensor was attached to the plate at a distance of 210 mm from the short side in order to exploit the maximum deformations as calculated by the FE model. No damping effect from the MFC sensor was considered in this paper.

In Figure 14 and Figure 15 are reported typical voltage signals acquired during the transition between the two stable states of the plates for the different boundary conditions represented in Figure 5.

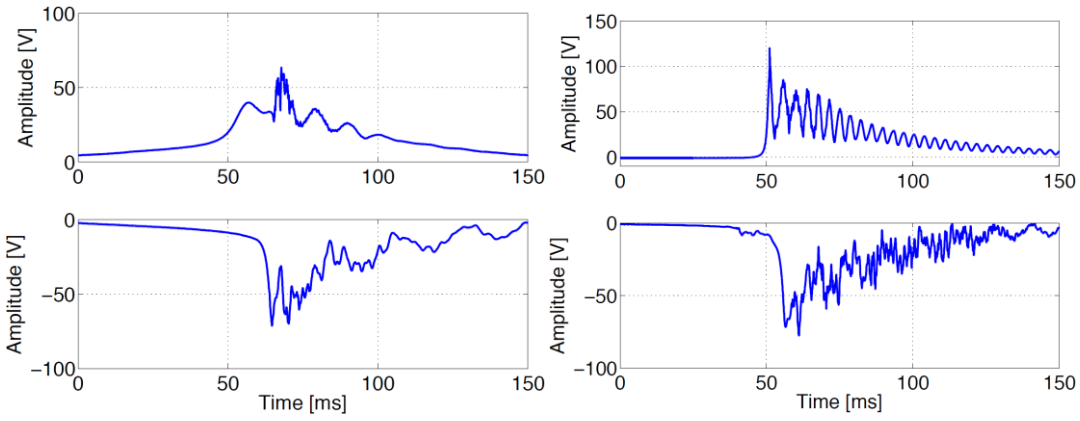

Figure 14: Reference supported configuration 1 (top: transition from stable state 1 to stable state 2; bottom: transition from stable state 2 to stable state 1).

Figure 15: Configuration with S=40 mm and L=240 mm (top: transition from stable state 1 to stable state 2; bottom: transition from stable state 2 to stable state 1).

During the acquisitions with the movable septum, the activation load was always applied at L = 240 mm. The plus or minus sign of voltage peak shows in which direction the MFC sensor is activated. It was found that the measured voltage depends on the combination of constraints and load application point since they influence the deformation at the point on the plate surface where the sensor is located. From Figure 14 and Figure 15, it is clear that the peaks of voltage amplitude decrease by increasing S. Therefore, the optimal configuration with S = 40 mm and L = 240 mm maximises the bistable deformation and, as a consequence, the voltage.

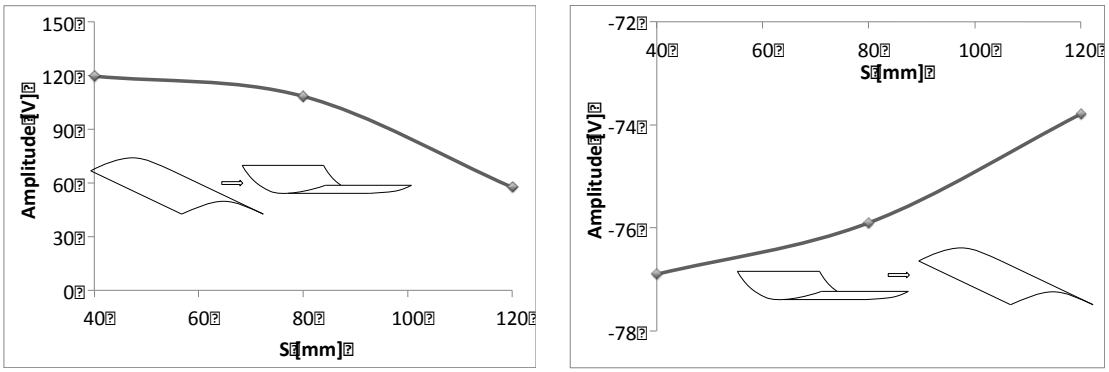

Figure 16: Voltage amplitude peak (L = 240 mm) (Left: transition from state 1 to state 2; Right: transition from state 2 to state 1).

To obtain the average power P_{avg} generated by a resistive load R during the snap-through process, the V_{RMS} (Voltage Root Mean Square) was used:

$$P_{avg} = \frac{V_{RMS}^2}{R} \tag{6}$$

where, in the case of a set of n values $\{v_1, v_2, \dots, v_n\}$ of the measured voltage, V_{RMS} is

$$V_{RMS} = \sqrt{\frac{1}{n}(v_1^2 + v_2^2 + \cdots + v_n^2)} \tag{7}$$

Voltage signals were acquired for the simply supported configuration 1 and the optimal lever configuration, assuming the same resistive load *R.* Hence the ratio between P_{avg} with and without the lever effect is proportional to the ratio of the squared V_{RMS}.

Simply supported Configuration		**Lever Configuration**				
Case 1	**Case 2**		**Case 1**		**Case 2**	
V_{RMS} [V]	**V_{RMS} [V]**	**S (mm)**	**V_{RMS} [V]**	**Power increase (%)**	**V_{RMS} [V]**	**Power increase (%)**
8.2113	**8.6624**	40	9.783	42 %	8.889	5 %
		80	9.410	31 %	8.787	3 %
		120	7.9125	-7 %	8.549	-3 %

Table 5: Performance of proposed power harvesting system (Case 1: transition from stable state 1 to stable state 2; Case 2: transition from stable state 2 to stable state 1).

In

Simply supported Configuration		**Lever Configuration**				
Case 1	**Case 2**		**Case 1**		**Case 2**	
V_{RMS} [V]	**V_{RMS} [V]**	**S (mm)**	**V_{RMS} [V]**	**Power increase (%)**	**V_{RMS} [V]**	**Power increase (%)**
8.2113	**8.6624**	40	9.783	42 %	8.889	5 %
		80	9.410	31 %	8.787	3 %
		120	7.9125	-7 %	8.549	-3 %

Table 5, the performance of the power harvesting system based on the bistable plate is evaluated taking as a reference the power generated on the simply supported configuration. This represents the traditional set-up for bistable power harvesting as

seen, for instance, in Potter et al. [14] and Arrieta et al. [11]. It is clear that the employment of the movable septum (lever configuration) improves the output power (up to 42%) when this is shifted towards the constrained edge. The improvement is higher for the transition from stable state 1 to stable state 2 (i.e. case 1) than the opposite (i.e. case 2). If the septum is moved towards the free edge of the plate, the improvement vanishes becoming even detrimental if this is moved too far (~-7%).

It should be noted that configuration 1 is the traditional one used in literature, and the results shown in

Simply supported Configuration		**Lever Configuration**				
Case 1	**Case 2**		**Case 1**		**Case 2**	
V_{RMS} [V]	**V_{RMS} [V]**	**S (mm)**	**V_{RMS} [V]**	**Power increase (%)**	**V_{RMS} [V]**	**Power increase (%)**
8.2113	**8.6624**	40	9.783	42 %	8.889	5 %
		80	9.410	31 %	8.787	3 %
		120	7.9125	-7 %	8.549	-3 %

Table 5 allow to assert that the lever effect improves the power harvesting performance with

8. Conclusions

A novel power harvesting system based on the “lever effect” was developed on a bistable composite panel in order to reduce the activation force for the snap-through transition. A multi-step finite element analysis allowed simulating both the cooling down

and the dynamic snap-through behaviour in order to study the mechanical deformations and activation forces as a function of the sample constraints. Experimental tests were carried out to characterise the bistable behaviour with different boundary conditions and to validate the numerical results using a specifically designed multifunctional sample holder. A micro fibre composite (MFC) sensor was surface attached on the composite plate to generate voltage peaks from the snap-through activation. The main outcomes of this research work are: (i) the activation forces responsible for the transition from one state to another are strongly dependent on the boundary conditions of the plate, and (ii) the septum position allows obtaining a "lever effect". Indeed, by maximising the distance between fulcrum and the load position it is possible to minimise the activation force. This reduction is of one order of magnitude with respect to simple supports assumed as a reference configuration of constraints. Particularly, it was found that the same configuration of septum and application load position minimises the activation forces of nearly 1 *N* and, at the same time, maximises the output energy (up to 42%). Therefore, a novel enhanced power harvesting system is here defined due to the high ratio between the output energy (related to the voltage provided by the sensor) and input energy (related to the activation force). These results are encouraging and this system could be furthermore exploited for future applications in energy harvesting using bistable structures.

References

[1] Harrist D., "Wireless battery charging system using radio frequency energy harvesting" Ph.D. thesis, 2004, Department of Electrical Engineering, University of Pittsburgh, Pittsburgh, PA.

[2] Amoroso F., Pecora R., Ferraro S., Lecce L., Girolami I., Antuonfermo P., "Design and testing of piezoelectric energy harvesting system from vibrations for wireless sensors", *Proceedings of 3rd CEAS Air&Space Conference*, Venice (Italy), October 2011, p. 1260-1269, ISBN: 9788896427187.

[3] Zhu D., Tudor M.J., Beeby S.P., “Strategies for increasing the operating frequency range of vibration energy harvesters: a review”, *Meas. Sci. Technol.* 21 (2010) 022001 (29pp).

[4] Harne R.L., Wang K.W., “A review of the recent research on vibration energy harvesting via bistable systems”, *Smart Material Structures*, 2013, doi: 10.1088/0964-1726/22/2/023001.

[5] Daqaq M. F., “Transduction of a bistable inductive generator driven by white and exponentially correlated Gaussian noise”, *J. Sound Vib. (2011) 330 2554–64.*

[6] Ferrari M., Ferrari V., Guizzetti M., Andò B, Baglio S., Trigona C., “Improved energy harvesting from wideband vibrations by nonlinear piezoelectric converters”, *Sensors and Actuators A: Physical, 2010, doi:10.1016/j.sna.2010.05.022.*

[7] Stanton Samuel C., McGehee Clark C., Mann Brian P., “Nonlinear dynamics for broadband energy harvesting: Investigation of a bistable piezoelectric inertial generator”, *Physica D,* 239 (2010) 640-653.

[8] Roundy S., Leland E., Baker J., Carleton E., Reilly E., Lai E., Otis B., Rabaey, Wright P., “Improving power output for vibration based energy scavengers”, *Pervasive Comput. IEEE*, 4 (1) (2005) 28-36.

[9] Andò,B. et al., “Magnetically-coupled cantilevers with antiphase bistable behavior for kinetic energy harvesting”, (2012) *Procedia Engineering*, 47, pp. 1065-1068.

[10] Arrieta A. F., Delpero T., Bergamini A. E., Ermanni P., “Broadband vibration energy harvesting based on cantilevered piezoelectric bi-stable composites”, *Applied Physics Letters* 102, 173904, 2013, doi: 10.1063/1.4803918.

[11] Arrieta A. F., Hagedorn P., Erturk A., Inman D. J., “A piezoelectric bistable plate for nonlinear broadband energy harvesting”, *Applied Physics Letters 97*, 104102 (2010), doi: 10.1063/1.3487780

[12] Inc. ANSYS. Workbench User’s Guide - Release 15.0, 2013.

[13] Hexcel Corporation Carbon/Epoxy. Data Sheet Composite T800/M21 Unidirectional Prepreg, 2012.

[14] Potter K. D., Daynes S., Diaconu C. G., Weaver P. M., “Bistable prestressed symmetric laminates”, *Composite Materials*, 44(9), 2010, doi: 10.1177/0021998309351603.

[15] Gauss K. F., “General Investigations of Curved Surfaces of 1827 and 1825”, The Princeton University Library, (1902).

[16] Gray A., Abbena E., Salamon S., “Modern Differential Geometry of Curves and Surfaces with Mathematica”, *Chapman & Hall/CRC*, (2006).

[17] Giddings P., Bowen C., Salo A., Kim H. A. and Ive A., “Bistable composite laminates: effects of laminate composition on cured-shape and response to thermal load”, *Composite Structures*, 92 (9), pp. 2220-2225, (2010).

[18] Abou Msallem Y., Jacquemin F., Boyard N., Poitou A., Delaunay D., Chatel S., “Material characterization and residual stresses simulation during the manufacturing process of epoxy matrix composites”, *Composites Part A: Applied Science and Manufacturing*, Volume 41, Issue 1, January 2010, Pages 108-115, ISSN 1359-835X, http://dx.doi.org/10.1016/j.compositesa.2009.09.025

[19] Hyer M.W., “The room-temperature shapes of four-layer unsymmetric cross-ply laminates”, *Journal of Composite Materials*, 1982, 16(4): p. 318-340.

[20] Hyer M.W., "Some observations on the cured shape of thin unsymmetric laminates", *Journal of Composite Materials*, 1981, 15(2): p. 175-194.

[21] Kim H.A., et al., "Shape memory alloy-piezoelectric active structures for reversible actuation of bistable composites". *AIAA Journal*, 48(6): p. 1265-1268, (2010).

[22] Wahied G. Ali, Sutrisno W. Ibrahim, "Power Analysis for Piezoelectric Energy Harvester", *Energy and Power Engineering* Vol.4 No.6(2012), Article ID:25084,10 pages doi:10.4236/epe.2012.46063.

[23] Yang, Y., Tang, L., & Li, H., "Vibration energy harvesting using macro-fiber composites", *Smart materials and structures*, 18(11), 115025, (2009).

[24] Sirohi J., Chopra I., "Fundamental Understanding of Piezoelectric Strain Sensors", *Journal of Intelligent Material Systems and Structures, Vol. 11 (2000) p. 246-257.* .

[25] Fuhong D., Li H. , "Finite Element Analysis of Multi-Stable Structures" chapter in *Finite Element Analysis - From Biomedical Applications to Industrial Developments*, Dr. David Moratal (Ed.),(2012) ISBN: 978-953-51-0474-2.

[26] Mattioni F., Weaver P.M., Potter K.D., Friswell M.I.. "Analysis of thermally induced multistable composites", *International Journal of Solids and Structures,* 45 (2008) 657–675, doi:10.1016/j.ijsolstr.2007.08.031

List of Figures

List of Tables